Steady-state *ab initio* theory of lasers with injected signals

Alexander Cerjan and A. Douglas Stone[*]

Department of Applied Physics, Yale University, New Haven, Connecticut 06520, USA

We present an *ab initio* treatment of the steady-state of lasers with injected signals that describes a regime, valid for microlasers, in which the locking transition is dominated by cross saturation and spatial hole burning. The theory goes beyond standard approaches and treats multimode lasing with injected signals and finds the possibility of partially locked states and as well as repulsion of the free-running frequencies from the injected signal. The theory agrees well with exact integration of the full wave and matter equations for the system. It can also describe accurately complex modern lasers structures and is applied to the example of deformed disk lasers. We show that in the case of a one-dimensional cavity in the locked or regenerative amplifier regime the theory reduces to an improved version of the Adler equations in the appropriate limit.

PACS number(s): 42.55.Px, 42.55.Ah, 42.60.Fc

I. INTRODUCTION

Laser action in the presence of an injected signal is an extremely important topic for research in both nonlinear dynamics and laser physics and for applications of lasers. Under certain conditions, a laser mode can be locked to the injection frequency, allowing for stabilization and modulation of a "slave" laser based on control by a "master" laser. This and related effects have been the topic of a large literature going back to the beginning of laser theory [1–4] and certain features are now well-described in textbook treatments [5], where the basic paradigm is that of frequency locking of nonlinear oscillators as described by Adler [6] well before the invention of the laser.

From the mid-1970s onward [7], it was also appreciated that lasers with injected signals can exhibit complex dynamical behavior and even chaos based on the general principle of nonlinear dynamics that damped driven nonlinear systems with three or more independent time-varying fields generically have nontrivial dynamics over large regions of phase space [8,9]. Since the basic laser equations involve three distinct and possibly complex functions (the electric field, the polarization, and the inversion amplitudes) a self-oscillating laser without injection can exhibit this behavior [7], but in most lasers the time scales are such that the polarization field (Class B) or the polarization and inversion (Class A) can be adiabatically eliminated and treated as functions of the other variables, leaving only one or two independent field(s).

Class B lasers are by far the most common type (they include semiconductor and most other solid state lasers), and so injecting an additional signal can in many cases generate interesting dynamical states outside the locking region. Hence Class B lasers with an injected signal have been used extensively to study such states in the past 30 years. Deterministic chaos was first reported in Class B lasers with injected signals by Arecchi *et al.* [10], who introduced the Class A, B, and C categories based on the relative size of the decay rates of the electric field, κ, polarization, $\gamma_\perp$, and inversion of the gain medium, $\gamma_\parallel$. (Class C is the case in which all time constants are comparable, none of the fields

can be adiabatically eliminated, and the laser in isolation can exhibit chaotic dynamics. These lasers are very rare and are not technologically important.) The goal of much of this earlier work has been to understand and categorize all of the different regimes of stability, bistability, and instability for injected class B lasers [10–15]. These interesting dynamical effects arise because the injected signal beats against the existing, free-running laser output and drives the inversion to oscillate at this beat frequency. When this frequency coincides with other relevant dynamical scales in the laser, usually the frequency of the relaxation oscillations, $\omega_r \sim \sqrt{\kappa\gamma_\parallel}$, resonant driving occurs, leading to complex dynamics. In addition, for semiconductor lasers, there are dynamical scales associated with the dispersion of the gain medium [16], and to carrier dynamics, which enter the equations as well; these effects arise from the real part of the gain susceptibility at the lasing frequency and are quantified by the Henry α factor [11,16–18].

In the current work we develop a theory of injection locking of Class A and B lasers in a regime relevant particularly to microlasers, in which complex dynamical states do not arise, and for atomiclike gain media for which the α factor is negligible. The existence of such a regime does not seem to have been clearly identified in previous work on injection locking. In this regime the physical effect is primarily that of quenching of the free-running laser oscillation due to cross saturation. There have been some relatively recent works [19,20] emphasizing locking through cross saturation as opposed to synchronization, but these models do not include spatial hole burning, which we find to play an important role, and the models also involve many more approximations than our method, which is essentially an exact solution of the problem in the relevant regime.

Our approach is a generalization of steady-state *ab initio* laser theory (SALT) which has previously been shown to provide extremely accurate solutions of the multimode laser equations, again in a regime relevant particularly to microlasers. SALT keeps the full space dependence of the electric field, polarization, and inversion and hence goes beyond the earlier treatments that led to the classifications A, B, and C, where these quantities were only functions of time. We retain this terminology to reference the hierarchy of time scales, but refer to the electric field, polarization, and inversion as fields. The accuracy of the generalized theory, injection-SALT, or

_____
[*]douglas.stone@yale.edu

I-SALT, is here confirmed by direct simulation of the relevant Maxwell-Bloch equations describing the laser with injected signal. In the limit where the laser is locked to the input signal we show that an approximate treatment of our theory reduces to an Adler type of steady-state solution, but that the behavior outside of the locking range is completely different than expected from the Adler description. Moreover, the Adler approximation is not very accurate for the phase difference between the locked input signal and the resulting amplified output.

To present I-SALT it is useful to review briefly SALT and the assumptions underlying that theory. SALT is based on a multiperiodic ansatz for the steady-state solutions of the semiclassical Maxwell-Bloch equations describing lasing. After transient effects have subsided it is assumed that the electric field in the laser cavity is a sum of some number, N_L, of unknown lasing modes, $\Psi_\mu(x)$, with unknown lasing frequencies, ω_μ, which are found by solving self-consistent coupled nonlinear frequency-domain wave equations (see below). These equations include space-dependent saturation of the gain and mode competition to infinite order. The number of lasing modes is not assumed to be known, but is also determined self-consistently from the theory, which predicts the thresholds including the effects of mode competition. The theory treats the openness of the cavity exactly through the introduction of a non-Hermitian basis set of outgoing functions, which are termed the threshold constant flux (TCF) basis and which will play a crucial role in I-SALT. The theory is also formulated for arbitrary cavity geometries and mode functions, so it is well suited to treat novel modern microlasers such as those based on disk, toroid, photonic crystal, or random cavities [21–24]. SALT is easily generalized to N-level lasing with a single lasing transition (not mode) and with minor complications can be applied to multiple lasing transitions and more complex gain media, as long as the basic approximation underlying the theory holds. The only substantial approximation in SALT is the neglect of the field beating terms in the multimode regime which can lead to complex dynamics and destabilize the multimode solution. This approximation leads to an inversion density which varies in space but not in time; hence, we refer to it as the stationary inversion approximation (SIA). By its nature, SALT and its generalization to I-SALT, will not describe complex dynamical effects in injected lasers of the type mentioned above.

However, as noted, there is an interesting regime in which such effects do not occur, and in which SALT and I-SALT will describe accurately the steady-state lasing or lasing with injection in either the locked or unlocked state. The theories will predict fully the classical fields, their frequencies, output power, emission pattern, etc., except properties due to quantum fluctuations, such as the linewidth. However, recent extensions of SALT [25,26] have found exact linewidth formulas which are generalizations of Schawlow-Townes based on SALT solutions. SALT without injection has been compared to full finite difference time domain (FDTD) simulations of microlasers using the Maxwell-Bloch and N-level semiclassical lasing equations and has been found to agree very well with a much reduced computational overhead. For higher dimensional structures and the full vector Maxwell equations SALT can be used where FDTD is computationally impractical [27,28].

II. VALIDITY OF SALT AND I-SALT

We now address the validity of the SIA which will define the regime of validity of multimode SALT and of I-SALT. A number of works in early laser theory rely on the SIA, including a seminal paper by Spencer and Lamb [4], which derives the Adler equations for the injected laser from the Maxwell equations with injection into a cavity with uniform gain. Most relevant to our work is that of Fu and Haken in 1991 [29], who argued that the SIA was valid and steady-state multimode operation was possible as long as $\gamma_\parallel, \kappa \ll \gamma_\perp, \Delta$, where $\gamma_\perp$ is the relaxation rate of the polarization and Δ is the free spectral range of the laser. They then studied a simplified model of a Fabry-Perot-type laser and showed that the multimode state with the largest number of modes was typically the stable state. They also pointed out that in order for $\Delta \gg \gamma_\parallel$ to hold, one typically would need to look at linear laser cavities of length $L \leqslant 100\ \mu m$.

Fu and Haken did not justify the requirement $\kappa \ll \gamma_\perp$ in their work and we find that through comparison with FDTD simulations the SIA and SALT work well even when $\kappa \geqslant \gamma_\perp$ ("bad cavity" limit). In the latter case the polarization cannot be adiabatically eliminated and does not follow the electric field instantaneously until steady state is reached; but in the steady state the SIA holds and the lasing fields are accurately determined by SALT. κ itself is not a relevant frequency scale for the validity of the SIA in the laser without injection; as long as $\gamma_\parallel \ll \gamma_\perp, \Delta$ the SIA, and hence SALT, will describe the steady-state. As noted above, the relaxation oscillation frequency, $\omega_r \sim \sqrt{\kappa \gamma_\parallel}$, can be relevant if it coincides with beat frequency of nearby modes, i.e., it is $\sim \Delta$, so that relaxing fluctuations could be resonantly enhanced and destabilize the multimode state. However, since $\kappa \leqslant \Delta$, $\omega_r \leqslant \sqrt{\Delta \gamma_\parallel} < \Delta, \gamma_\perp$ (we assume that in the interesting cases $\gamma_\perp \geqslant \Delta$; otherwise multimode lasing is unlikely, since $\gamma_\perp$ is the width of the gain curve). So for steady-state multimode lasing without injection all that is required for our free-running theory to work is $\gamma_\parallel \ll \gamma_\perp, \Delta$.

For the injected laser the inversion beat frequency is not Δ, but the frequency difference between the injected signal ω_{in} and the free-running signal ω_1 (we assume here only one free-running mode and one injected signal for simplicity). For the generalization to I-SALT to work in the unlocked regime, where there are two beating signals, we must have $\omega_{in} - \omega_1 > \omega_r$. However, even if this is not the case, I-SALT will still describe quantitatively the locked regime and predict the unlocking threshold exactly.

In the cases studied below, in which I-SALT describes both the locked and the unlocked behaviors, we find an effect in 1D Fabry-Perot-type cavities: Instead of the free-running frequency being "pulled in" to the injected frequency, as in the standard Adler picture [5], we find that the lasing frequency is repelled from the injected signal frequency due to the effects of gain competition and spatial hole burning. In Oppo *et al.* frequency repulsion is also found in a certain limit, but it is due to the dynamical effects of relaxation oscillations which are absent for the cases we consider and thus is a distinct effect. Moreover, essentially all of the injection literature treats single-mode one-dimensional cavities. I-SALT naturally allows the description of multimode lasing with injection, leading to the

possibility of a partially locked lasing state, in which one or more modes have been quenched by cross saturation, while other modes still lase, as we demonstrate below. Also, I-SALT provides a formulation for describing injection into a cavity with arbitrary two- or three-dimensional geometry; we apply the method to injection into a two-dimensional chaotic cavity laser below.

The outline of this paper is as follows. In Sec. III we derive I-SALT using a convenient basis in which to express the problem, which also facilitates its solution numerically. In Sec. IV we derive a version of the Adler steady-state theory from I-SALT, valid for relatively high-Q cavities. In Sec. V we present numerical results comparing I-SALT to direct integration of the Maxwell-Bloch equations in time and demonstrate excellent agreement in the regime of relatively low-Q cavities where we expect other approaches to fail. This section also demonstrates the frequency repulsion of the lasing mode from the injected mode, in contrast to predictions of previous theories. We also present here a comparison between the I-SALT version of the Adler equation in the locked regime and full I-SALT for higher Q cavities. Finally, we present an application of I-SALT to injection locking in two-dimensional cavities. In Sec. VI we summarize and make some concluding remarks.

III. DERIVATION OF I-SALT

As introduced above, SALT was formulated to determine directly the steady state of the laser rate equations for an N-level atomic gain medium coupled to Maxwell's equations within an arbitrary cavity specified by its passive dielectric function, a tensor in general, $\varepsilon_c(\mathbf{x})$, and subject to a spatially varying pump, $D_0(\mathbf{x}) = d_0 F(\mathbf{x})$, without performing time integration to steady state. Assuming stationary level populations (stationary inversion for the two-level medium), a multimode steady state exists and is described by a set of time-independent wave equations coupled through their nonlinear saturation terms and subject to the non-Hermitian boundary condition of purely outgoing solutions at the lasing frequencies. The SALT equations are solved efficiently by introducing a specific self-orthogonal basis set of TCF states in which to expand the solutions and then iteratively solving the resulting nonlinear matrix equation for both fields and frequencies. We now show how this approach can be generalized to yield I-SALT.

The Maxwell-Bloch equations, which describe the coupling of the electric field to a population of two-level gain atoms [7],

$$4\pi \partial_t^2 \mathbf{P}^+ = c^2(\nabla \times \nabla \times \mathbf{E}^+) - \varepsilon_c(\mathbf{x})\partial_t^2 \mathbf{E}^+ \qquad (1)$$

$$\partial_t \mathbf{P}^+ = -(\gamma_\perp + i\omega_a)\mathbf{P}^+ + \frac{\mathbf{g}}{i\hbar}D(\mathbf{E}^+ \cdot \mathbf{g}) \qquad (2)$$

$$\partial_t D = -\gamma_\parallel[D - d_0 F(\mathbf{x})] - \frac{2}{i\hbar}[\mathbf{E}^+ \cdot (\mathbf{P}^+)^* - (\mathbf{E}^+)^* \cdot \mathbf{P}^+], \qquad (3)$$

form the basis for SALT. In these equations $\mathbf{E}^+$ and $\mathbf{P}^+$ are the positive frequency components of the electric field and atomic polarization, respectively, ω_a is the atomic transition frequency, and $\mathbf{g} = e\langle e|\hat{\mathbf{x}}|g\rangle$ is the dipole matrix element in which $|e\rangle$ and $|g\rangle$ are the excited and ground spatial states

of the electron wave functions. In separating the electric field into its positive and negative frequency components, terms oscillating at twice the atomic frequency have been omitted, corresponding to the usual rotating-wave approximation (RWA). Note that we have not introduced the slowly varying envelope approximation for the electric field as is usually done; this is unnecessary for the steady-state and provides no computational advantage. As noted above, it has been previously demonstrated that any N-level atomic medium with a single lasing transition in the steady state can be reduced to an effective two-level atomic system of the type considered here in the steady-state limit [27]. Furthermore, SALT has also been shown to describe more complex gain media (C-SALT), which have multiple lasing transitions and diffusion of the gain atoms [30], as long as the SIA still holds. However, for simplicity, in this paper we focus only on the Maxwell-Bloch equations as written above.

As discussed above, we assume the existence of a steady state with stationary level populations, which in general requires that $\gamma_\parallel, \omega_r \ll \delta\omega, \Delta, \gamma_\perp$, where $\delta\omega$ is the detuning of the injected signal from the free-running laser frequency and $\omega_r, \Delta, \gamma_\perp$ are as previously defined. However, for a cavity with only a single operating mode, either injected or free-running, this inequality is not necessary, and the I-SALT solution is exact (in the RWA). In general, the positive frequency components of the electric field and atomic polarization inside the cavity for a given pump value, d_0, take the form

$$\mathbf{E}^+(\mathbf{x},t) = \sum_\mu^{N_L} \Psi_\mu(\mathbf{x})e^{-i\omega_\mu t} + \sum_\alpha^{N_A} \Psi_\alpha(\mathbf{x})e^{-i\omega_\alpha t}, \qquad (4)$$

$$\mathbf{P}^+(\mathbf{x},t) = \sum_\mu^{N_L} \mathbf{p}_\mu(\mathbf{x})e^{-i\omega_\mu t} + \sum_\alpha^{N_A} \mathbf{p}_\alpha(\mathbf{x})e^{-i\omega_\alpha t}, \qquad (5)$$

where the N_L lasing modes, $\Psi_\mu(\mathbf{x})$, and associated polarization fields, $\mathbf{p}_\mu(\mathbf{x})$, have unknown spatial variation, and unknown frequencies, ω_μ, and there are N_A amplified signals injected into the cavity, at *given* frequencies, ω_α, and *given* incoming amplitudes, B_α, but with unknown overall amplitude, spatial variation, $\Psi_\alpha(\mathbf{x})$, and polarization, $\mathbf{p}_\alpha(\mathbf{x})$, within the cavity. All of the unknown quantities are determined from the resulting I-SALT equations and their boundary conditions self-consistently. We now insert the multiperiodic ansatz (4) and (5) into the Maxwell-Bloch equations and apply the SIA to write

$$\mathbf{p}_\sigma(\mathbf{x}) = \frac{\mathbf{g}}{\hbar}\frac{D(\mathbf{x})}{\omega_\sigma - \omega_a + i\gamma_\perp}[\Psi_\sigma(\mathbf{x}) \cdot \mathbf{g}], \qquad (6)$$

where σ is either a free-running or an injected mode. This allows for the elimination of the polarization and atomic inversion, leading to $N_L + N_A$ coupled nonlinear wave equations, which can be written as three-dimensional vectorial equations, but which here we only consider in their scalar form, appropriate for the geometries

$$\left\{\nabla^2 + \left[\varepsilon_c(x) + \frac{\gamma_\perp D(x)}{\omega_\sigma - \omega_a + i\gamma_\perp}\right]k_\sigma^2\right\}\Psi_\sigma(x) = 0, \qquad (7)$$

$$D(x) = \frac{d_0 F(x)}{1 + \sum_\mu^{N_L} \Gamma_\mu|\Psi_\mu(x)|^2 + \sum_\alpha^{N_A} \Gamma_\alpha|\Psi_\alpha(x)|^2}, \qquad (8)$$

where $\Gamma_\sigma \equiv \gamma_\perp^2/[(\omega_\sigma - \omega_a)^2 + \gamma_\perp^2]$ is the gain curve and $k_\sigma = \omega_\sigma/c$ is the wave vector. The electric field and inversion have also been scaled to natural units, $E_c = 2g/\hbar\sqrt{\gamma_\parallel\gamma_\perp}$ and $D_c = 4\pi g^2/\gamma_\perp\hbar^2$. The wave equations for lasing modes, $\Psi_\mu(x)$, are to be solved with purely outgoing boundary conditions, while those for amplified modes, $\Psi_\alpha(x)$, are to be solved with the boundary condition of fixed input amplitude B_α at ω_α.

We solve these coupled equations by nonlinear iteration after expanding the solutions in a non-Hermitian basis set with the appropriate boundary conditions. For the lasing modes, Ψ_μ, this set is the same TCF states used in SALT, which satisfy

$$\{\nabla^2 + [\varepsilon_c(x) + \eta_n F(x)]k^2\}u_n(x;\omega) = 0, \tag{9}$$

$$\partial_x u_n(x;\omega)|_{x=L} = iku_n(L;\omega), \tag{10}$$

$$u_n(0;\omega) = 0, \tag{11}$$

where we refer to $u_n(x;\omega)$ and $\eta_n(\omega)$ as the TCF eigenvectors and eigenvalues, respectively, and we have written the outgoing boundary condition explicitly for a one-sided cavity with a perfect mirror at the origin of the type we study below. The general outgoing boundary condition is expressed differently for different geometries, but is well known. Note that $\{\eta_n(\omega)\}$ is generically complex and can be thought of as the set of values of the gain medium susceptibility which lead to lasing at frequency ω, i.e., for which a solution for purely outgoing real wave vector exists [31]. In this basis the lasing mode is written as

$$\Psi_\mu(x) = \sum_n a_n^{(\mu)} u_n(x;\omega_\mu). \tag{12}$$

Thus, the lasing thresholds in the absence of input signals are obtained by varying ω in the TCF equation until a frequency, ω_μ, is found at which

$$\eta_n(\omega_\mu) = \frac{d_0\gamma_\perp}{\omega_\mu - \omega_a + i\gamma_\perp}. \tag{13}$$

The $\{u_n(x;\omega_\mu)\}$ then form an efficient basis set for finding the *nonlinear* solutions above threshold because at the first lasing threshold, the lasing mode is only a single TCF state, and above threshold only a small number of TCFs are needed to converge to the nonlinear solution of the SALT equations.

The amplified modes, Ψ_α, however, must be treated differently from the lasing modes since they have a fixed incoming signal amplitude and fixed frequency. To represent these modes we require terms with an incoming component in addition to the outgoing TCF expansion terms, which we do conveniently by solving the same TCF equation inside the cavity with a purely incoming boundary condition,

$$\Psi_\alpha(x) = \sum_n a_n^{(\alpha)} u_n(x;\omega_\alpha) + \sum_m b_m^{(\alpha)} v_m(x;\omega_\alpha), \tag{14}$$

where the states $v_m(x;\omega)$ and associated eigenvalues β_m are given by

$$\{\nabla^2 + [\varepsilon_c(x) + \beta_m F(x)]k^2\}v_m(x;\omega) = 0, \tag{15}$$

$$\partial_x v_m(x;\omega)|_{x=L} = -ikv_m(L;\omega), \tag{16}$$

$$v_m(0;\omega) = 0, \tag{17}$$

and thus represent states that are purely incoming. The incoming and outgoing TCF states are not power orthogonal, but they do satisfy a self-orthogonality condition between themselves,

$$\frac{1}{L}\int_C dx\, F(x)u_n(x;\omega)u_m(x;\omega) = \delta_{nm}, \tag{18}$$

$$\frac{1}{L}\int_C dx\, F(x)v_n(x;\omega)v_m(x;\omega) = \delta_{nm}, \tag{19}$$

which can be derived from the definitions of the states and Green's theorem. Either the incoming or the outgoing TCF states represent a complete basis for fields *within the cavity* at ω_α, but the incoming terms are needed to represent the input boundary condition. Because they are purely incoming, they do not contribute directly to the emitted fields, but they correctly represent the full spatial hole-burning and gain competition effects of the amplified input.

For amplified modes, we can easily write the incoming boundary condition for a one-sided slab cavity of length L as

$$B_\alpha e^{-ik_\alpha L} = \sum_m b_m^{(\alpha)} v_m(L;\omega_\alpha), \tag{20}$$

where B_α is the given incoming field amplitude at frequency ω_α. This single equation vastly underdetermines the coefficients $b_m^{(\alpha)}$ in the sum, so that the choice is based on convenience. This freedom arises from the overcompleteness of using both $\{u_n\}$ and $\{v_m\}$ to represent the internal fields. Hence, the coefficients $a_n^{(\alpha)}$ depend strongly on the choice of the $b_m^{(\alpha)}$. A natural choice is to take only a single term, $v_0(x;\omega_\alpha)$, which corresponds to the dominant component of the outgoing TCF state for the nearest lasing mode. This is allowed for a cavity with a single input channel, as in the one-sided slab geometry we are considering here; in general, one needs a minimum of M independent incoming states to represent an arbitrary input for an M-channel cavity, and these can be chosen again to be similar in character to the nearest lasing mode in order to optimize the calculation.

Once a representation of the input field is chosen, one can insert the expansions (14) for the amplified modes and (12) for the lasing modes into the fundamental Eqs. (7) and (8) and use the self-orthogonality relations of the outgoing TCF states to find coupled nonlinear matrix equations for the coefficients $a_n^{(\mu)}, a_n^{(\alpha)}$ which determine their solutions. For the lasing modes, Ψ_μ, one finds

$$\eta_l a_l^{(\mu)} = \sum_n T_{ln}^{(\mu)} a_n^{(\mu)}, \tag{21}$$

$$T_{ln}^{(\mu)} = \frac{\gamma_\mu d_0}{L}\int_C dx\, \frac{F(x)u_l(x;\omega_\mu)u_n(x;\omega_\mu)}{1 + \sum_\sigma^{(N_L+N_A)} \Gamma_\sigma|\Psi_\sigma(x)|^2}, \tag{22}$$

where $\gamma_\mu = \gamma_\perp/(\omega_\mu - \omega_a + i\gamma_\perp)$. This is identical to the lasing equations of SALT except for the presence of the amplified mode intensities in the nonlinear hole-burning denominator.

In a similar manner the coupled equations for the amplified modes can be determined, and they take the form

$$\eta_l a_l^{(\alpha)} = \sum_n T_{ln}^{(\alpha)} a_n^{(\alpha)} + \sum_m \left(W_{lm}^{(\alpha)} + V_{lm}^{(\alpha)} \right) b_m^{(\alpha)}, \quad (23)$$

$$W_{lm}^{(\alpha)} = \frac{\gamma_\alpha d_0}{L} \int_C dx \, \frac{F(x) u_l(x; \omega_\alpha) v_m(x; \omega_\alpha)}{1 + \sum_\sigma^{(N_L + N_A)} \Gamma_\sigma |\Psi_\sigma(x)|^2},$$

$$V_{lm}^{(\alpha)} = \frac{\beta_m}{L} \int_C dx \, F(x) u_l(x; \omega_\alpha) v_m(x; \omega_\alpha). \quad (24)$$

The result for the overlap integral can be simplified further through the use of the definitions of the incoming and outgoing TCF states and Green's theorem, allowing one to write

$$V_{lm}^{(\alpha)} = \frac{2i}{Lk_\alpha} \frac{\beta_m}{\beta_m - \eta_l} u_l(L; \omega_\alpha) v_m(L; \omega_\alpha). \quad (25)$$

As with any basis expansion method, this method of representing the original differential equations will require truncation of the sums at a finite number of TCFs, N, in the numerical implementation.

From this form of the overlap integral, it is simple to understand why the most numerically efficient choice of incoming TCF states to use, $b_m^{(\alpha)} \neq 0$, are those related to the outgoing states of the nearest lasing mode. In the case of a lossless cavity, $\varepsilon_c(x) \in \mathbb{R}$, the incoming and outgoing TCF states form a biorthogonal set, with $\beta_m = \eta_m^*$ and $v_m = u_m^*$. Thus, V_{lm} is maximized when the difference between the incoming and outgoing TCF eigenvalues is minimized. This choice allows the outgoing states required by T_{ln} to also have significant overlap with the incoming states chosen, rather than needing to include additional outgoing states to properly compute the sum over overlap integrals.

The I-SALT equations for free-running modes (21) and (22) have a critical difference from the equations for amplified modes (23)–(25): In the former, there is an undetermined global phase, whereas for the latter the phase is set by the injected signal, B_α. For lasing modes the undetermined global phase is chosen by convention (gauge condition) [31,32]. This leaves $2N - 1$ expansion coefficients to fully determine the real and imaginary parts of $a_n^{(\mu)}$, and one additional equation which determines the unknown lasing frequency. It is this equation which determines the full intensity-dependent line-pulling effects on the lasing frequencies, and, in the case of I-SALT, frequency pulling or pushing due to the injected mode. In contrast, for the amplified mode the frequency and phase of the input signal is fixed externally and uniquely determines all other phases (there is no global phase invariance); thus, there are $2N$ expansion coefficients (the real and imaginary parts of $a_n^{(\alpha)}$) that must be found, and an equal number of conditions determining them.

Together Eqs. (21)–(25) define I-SALT. In the regime in which the SIA holds, they provide essentially exact solutions of the full coupled wave equations for amplification and injection locking. The method is *ab initio*, as in SALT, with no prior assumptions about the number, spatial form or frequencies of the lasing modes. Lasing modes correspond to poles of the nonlinear scattering matrix on the real axis. Amplified inputs do not; they are simply additional scattered waves which also deplete the gain. If the input signal becomes too strong, and is sufficiently near in frequency to the lasing mode, then the lasing mode has insufficient gain and falls below threshold, leaving only the amplified signal output. The output is "locked"

to the input frequency, but not by pulling the lasing mode over to ω_α, but rather by turning it off.

IV. FROM I-SALT TO ADLER'S MODEL

In this section we show how I-SALT can recover an improved version of the traditional Adler equations in their steady-state form. Because our approach starts from the full laser equations we use as comparison Eqs. (58) and (59) from Spencer and Lamb [4], which has a similar starting point (i.e., starts with the full Maxwell equations and includes the spatial degrees of freedom and gain saturation explicitly). The Adler theory assumes only a single input channel with small amplitude and only, at most, a single free-running mode and a single amplified mode; we model the injected laser following Spencer and Lamb via a cavity with a perfect mirror at one end and a high-reflectivity mirror at the other. I-SALT is a steady-state theory and should only approach the Adler description in the locked regime; thus, we assume that only a single, highly amplified mode is present in the cavity. This allows us to approximate the field inside the cavity as only having two components, one incoming TCF and one outgoing TCF (instead of the full expansion in outgoing TCFs),

$$\Psi_{\text{in}}(x) = au(x; \omega_{\text{in}}) + bv(x; \omega_{\text{in}}), \quad (26)$$

with $a \gg b$ and where ω_{in} is the frequency of the incident signal. In a single-channel cavity the use of a single incoming TCF is always justified and in a high-Q cavity the use of a single outgoing TCF is justified by the single pole approximation (SPA) [31], as the amplified signal is close to a high-Q cavity resonance and thus only a single outgoing TCF is needed to describe the amplified mode in this limit. We can use Eqs. (9) and (15) to rewrite Eq. (7) as

$$\frac{\gamma_\perp D(x)}{\omega_{\text{in}} - \omega_a + i\gamma_\perp} \Psi_{\text{in}}(x) = a\eta_{\text{in}} u(x) + b\beta_{\text{in}} v(x), \quad (27)$$

$$D(x) = \frac{D_0}{1 + \Gamma_{\text{in}} |\Psi_{\text{in}}(x)|^2}. \quad (28)$$

By adding and subtracting $b\eta_{\text{in}} v(x)$ from the right side of the equation and defining $\Psi_{\text{in}}(x) \equiv a\psi(x)$, we are able to write

$$\frac{\gamma_\perp D(x)}{\omega_{\text{in}} - \omega_a + i\gamma_\perp} a\psi(x) - a\eta_{\text{in}} \psi(x) = b(\beta_{\text{in}} - \eta_{\text{in}}) v(x). \quad (29)$$

While Spencer and Lamb used a δ-function index jump to represent the imperfect mirror, for convenience we take our cavity to have a uniform index with the index step at one end to vacuum, comprising the mirror; hence, the TCF states will be sine functions of a complex argument. Thus, in this section only, we choose to normalize our incoming and outgoing TCF states for convenience as $(2/L) \int dx u(x) u(x) = 1$ and similarly $(2/L) \int dx v(x) v(x) = 1$. Integrating through with respect to the mode describing the resonance of the cavity, $(2/L) \int dx u(x)$, we define the gain saturation function as

$$f(I) = \frac{\omega_{\text{in}} D_0}{2\varepsilon_c} \left(\frac{2}{L} \right) \int dx \, \frac{u(x)\psi(x)}{1 + \Gamma_{\text{in}} I |\psi(x)|^2}, \quad (30)$$

where $I \simeq |a|^2$ is a measure of the intensity of the field inside of the cavity, and has essentially the same meaning as the

similar quantity introduced in Spencer and Lamb (in their case they use a sine of real argument and are able to evaluate the resulting integral analytically) [4]. Although $f(I)$ is complex in general, for high-Q cavities, it is essentially real to 10^{-3}, and thus here we approximate it as such. Next, we note that up to corrections of order b/a, $(2/L) \int u(x)\psi(x)dx = 1$ as the field profile inside of the cavity is dominated by the outgoing portion. Finally, the overlap integral between the incoming and outgoing TCF states can be evaluated by use of Eq. (25), resulting in

$$\frac{\gamma_\perp f(I)}{\omega_{\rm in} - \omega_a + i\gamma_\perp}\left(\frac{2\varepsilon_c}{\omega_{\rm in}}\right)a - \eta_{\rm in}a = \frac{2ic}{\omega_{\rm in}}\left(\frac{2}{L}\right)u(0)B_{\rm in},$$

(31)

where the mirrored side of the cavity has been placed at $x = -L$ and the open edge of the cavity at $x = 0$ and noting that the definition of the input signal amplitude, Eq. (20), can be used to simplify $B_{\rm in} = bv(0)$. The outgoing TCF eigenvalue for a dielectric slab cavity can be expressed in terms of the input frequency and the cavity resonance, following Ge et $al.$ [31],

$$\eta_{\rm in} = \varepsilon_c\left[\frac{\left(\omega_0 - i\frac{\gamma_c}{2}\right)^2 - \omega_{\rm in}^2}{\omega_{\rm in}^2}\right]$$

$$\simeq \varepsilon_c\left[\frac{2(\omega_0 - \omega_{\rm in})}{\omega_{\rm in}} - \frac{2i}{\omega_{\rm in}}\left(\frac{\gamma_c}{2}\right)\right],$$

(32)

where ω_0 is the frequency of the passive cavity resonance, γ_c is the photon decay rate through the end of the cavity, and $\omega_0 \simeq \omega_{\rm in}$, as the resonance corresponds to the closest passive cavity resonance to the injected frequency, at most half a free spectral range away. Finally, we approximate $(\omega_{\rm in} - \omega_a)^2 \simeq 0$, resulting in

$$(\xi - i)f(I)a - \left(\Delta - i\frac{\gamma_c}{2}\right)a = \frac{2ic}{L\varepsilon_c}u(0)B_{\rm in},$$

(33)

where $\xi = (\omega_{\rm in} - \omega_a)/\gamma_\perp$ and $\Delta = \omega_0 - \omega_{\rm in}$. In high-$Q$ cavities with the normalization for the outgoing TCFs chosen in this section, it can be shown that $u(0) \simeq 1$. The cavity decay rate can also be related to the round trip time in the cavity and the reflection coefficient [5],

$$\gamma_c = \frac{-c}{2Ln}\ln R,$$

(34)

where n is the index of refraction of the passive cavity. Finally, to connect to the Spencer and Lamb version of the Adler theory, we formally expand the reflection coefficient for large index, approximating the coefficient, $-\ln R \approx T \approx 4/n$, resulting in

$$\gamma_c \approx \frac{2c}{L\varepsilon_c}.$$

(35)

Finally, writing $B_{\rm in} = |B_{\rm in}|e^{i\phi}$ and separating real and imaginary components, we find

$$0 = \left[f(I) - \frac{\gamma_c}{2}\right]a - \gamma_c|B_{\rm in}|\cos(\phi),$$

(36)

$$0 = \xi f(I) - \Delta - \gamma_c\frac{|B_{\rm in}|}{a}\sin(\phi).$$

(37)

Noting that in the locked regime $\omega = \omega_{\rm in}$, Eqs. (36) and (37) are identical to the steady-state Adler equations as presented in

Eqs. (58) and (59) from Spencer and Lamb [4], except that our definition of $f(I)$ includes the openness of the cavity through different boundary condition on the TCF state, leading to a sine function of complex argument, instead of the Dirichlet boundary condition assumed in [4].

Thus, in the correct limit, an improved version of the traditional theory can be recovered from I-SALT, in the locked regime. If we make the further usual assumption that ξ is small, we obtain exactly the same locking range as predicted by the standard theory (see next section). In the unlocked regime the Adler theory predicts a residual time dependence of the relative phase of input and free-running signal which cannot be derived from I-SALT; but full I-SALT shows that the frequency shifts predicted by the usual theory in the unlocked regime are not correct in general (next section).

V. NUMERICAL RESULTS

To test the results of I-SALT, we compare them to the exact numerical solutions from FDTD simulations of the Maxwell-Bloch equations for a simple one-dimensional asymmetric Fabry-Perot cavity with an injected signal (schematics) under various conditions. The FDTD simulations performed here used the time-stepping method proposed by Bidégaray, updating the atomic polarization and inversion alongside the magnetic field and were run for a total time of $T_{\rm tot} \sim 100(1/\gamma_\parallel)$ to ensure convergence, as $\gamma_\parallel$ corresponds to the longest time scale in the system [33]. Similar simulations without the injected signal were previously used for quantitative tests of SALT [27,34].

A. locking transition

We first study the usual locking transition in Fig. 1 in which a single free-running mode eventually gives way to an injected mode. The simulations are done in a region of large detuning in which we expect good agreement with I-SALT. Indeed locking of the output signal to the input is found in the FDTD data in good quantitative agreement with I-SALT with no adjustable parameters. We note that the quantitative agreement seen between I-SALT and FDTD calculations is also a demonstration of the stability of the I-SALT solutions; any instabilities due to beating terms in the inversion would be present in the FDTD solutions, which do not rely on the SIA. A further analytical treatment of the stability of the I-SALT solutions is presented in the Appendix. The simulations in Fig. 1 are for large detuning, not the typical Adler regime; thus, for these parameters locking requires an input signal which is a significant fraction of the free-running output at that pump value, ~23%. The total output intensity of the amplified mode when locking occurs is larger than the free-running signal also by ~18% (in the Adler theory they are the same to a good approximation); however, this is not surprising due to the relatively large input intensity. Also, the independence of the spatial degrees of freedom of the amplified and free-running mode should allow the amplifier to extract more power from the gain medium. Consistent with this, in the unlocked region, when both free-running and amplified modes are emitting, the total output intensity is monotonically increasing, as indicated by the black dashed line in the figure. If we take the I-SALT
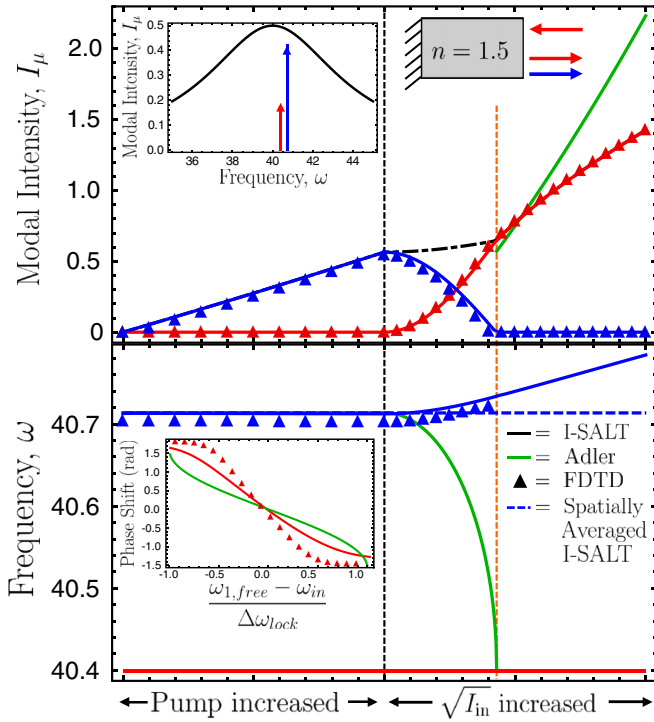
FIG. 1. (Color online) (Top) Simulations of single-mode injection locking in a one-sided dielectric slab cavity with $n = 1.5$ (schematic) with a perfect mirror at one end and an index step to vacuum at the other. First, the pump is increased above the threshold for lasing at $\omega_{1,\text{free}} = 40.714$, $D_0 = 0.0603$ to $D_0 = 0.08$, and then held at a fixed value (vertical black line) while the input signal amplitude is ramped from $B_{\text{in}} = 0$ until the free-running signal is quenched and the system "locks" (vertical orange line) to the injected frequency, $\omega_{\text{in}} = 40.4$ at $B_{\text{in}} = 0.176$. Finally, the simulation is continued in the locked regime to $B_{\text{in}} = 0.4$. Solid lines are output intensities calculated from I-SALT; blue is lasing output, red is amplified output at signal frequency, dot-dashed black is total output. Triangles are the same quantities from FDTD for the same dielectric slab laser with $\omega_a = 40$, the width of the gain curve, $\gamma_\perp = 4$, and $\gamma_\parallel = 0.001$. The green curve in the locked regime is the prediction of our generalized Adler equations, (36) and (37). The top inset shows gain curve and ω_{in} (red), ω_1 (blue). (Bottom) Frequency variation of the first lasing mode. Tlue line is from I-SALT and blue triangles from FDTD. The green line shows the prediction of the Adler theory. The red line is the injected signal frequency. Again, the orange dashed line shows the locking threshold from I-SALT; frequencies beyond this point are taken as the real part of the location of the pole of the scattering matrix. As the locking transition is approached, the lasing frequency moves *away* from the injected frequency, due to spatial hole burning instead of being attracted toward it, as expected from the Adler equation [5]. Blue dashed lines showing negligible frequency shift are I-SALT calculation with uniform gain saturation and no spatial hole burning. The inset shows a plot of the phase shift between input and output signals of an injection-locked dielectric slab cavity at a fixed input intensity. I-SALT (red curve) and FDTD simulations (red triangles) are seen to have a better quantitative and qualitative agreement than the Adler prediction (green curve). For comparison with the Adler theory, the horizontal axis is plotted in terms of the free-running lasing frequency in the absence of an injected signal at threshold, $\omega_{1,\text{free}}$. Frequencies and rates are given in units of c/L, while the atomic inversion and modal intensities are given in SALT units of E_c and D_c.

version of the Adler equations in the locked regime and impose the condition that locking occurs when the amplified output is equal to the original free-running output, we can solve the nonlinear Eqs. (36) and (37) to predict the input amplitude at which the laser would lock. This transition line is very close to that found by I-SALT, slightly less by $\sim 4.5\%$. Above that point we can plot the Adler I-SALT predictions for the amplified mode intensity and find them to be in reasonable agreement with I-SALT and FDTD near the transition and in poor agreement far above it.

The difference between the locking behavior in this regime and in the usual Adler theory is strikingly illustrated by the frequency shift of the free-running mode prior to locking, which is qualitatively different from the Adler theory; the free-running frequency, ω_1, is repelled from the input frequency (full blue line and data points), instead of being strongly attracted toward it (green line). This frequency repulsion can be explained by the combined effects of mode competition and spatial hole burning. As the incident signal is imposed and depletes the gain, the standing wave of the laser field shifts away from the frequency/wavelength of the incident standing wave in order to better extract energy from the regions of the cavity where the gain is not being saturated by the incident signal. To confirm this interpretation we replaced the *space-dependent* gain saturation denominator with its spatial average,

$$D_{\text{ave}}(x) = \frac{d_0}{1 + \sum_\sigma^{N_L + N_A} \frac{\Gamma_\sigma}{L} \int_C |\Psi_\sigma(x)|^2 dx}, \qquad (38)$$

in place of Eq. (8), and noting that for this simulation the pump profile is uniform, $F(x) = 1$. Using this spatially averaged gain saturation, no movement of the lasing frequency is seen in Fig. 1(b) (dashed blue line). This provides strong evidence that the frequency pushing phenomenon observed here requires treating the full spatial dependence of the problem and can not be seen in previously developed spatially averaged injection theories [12–14].

Furthermore, as I-SALT and FDTD simulations both predict this same frequency repulsion and this solution is found to be stable (see the Appendix), the effect seen here is different from the frequency repulsion previously predicted in dynamical parameter regimes by Oppo *et al.*, where the SIA would not be appropriate and as a result more complex dynamical features are found [12]. The relatively weak repulsion found here is also distinct from that observed by Murakami *et al.* [35], which is a shift in the cavity resonance due to the injected signal saturating the gain carriers in materials with large Henry α-factors such as semiconductors where $\alpha \sim 2$–8. In contrast, for the Bloch gain medium used in Fig. 1, $\alpha = 0.17$. Additionally, the overall saturation of the gain medium is not changing significantly while this frequency repulsion is observed as the pump is held fixed while the injected signal is increased, thus keeping the total output intensity relatively constant, as is seen in Fig. 1(a) in the black dot-dashed line. For the effect predicted by Murakami *et al.* to be seen, a significant shift in the number of available gain carriers is needed, coupled to a large Henry α-factor, and this effect would be seen in the spatially averaged I-SALT calculation if it were present [35].

As noted, the Adler theory describes locking driven by phase synchronization of the input and free-running fields. Since the threshold input intensity for locking decreases to zero as the input frequency, $\omega_{\rm in}$, approaches the free-running frequency in the absence of an injected signal, $\omega_{1,\rm free}$, the threshold condition can be expressed as a "locking range," the frequency range $\Delta\omega_{\rm lock}$ over which the laser is locked for a given input intensity. In the Adler theory one finds

$$\Delta\omega_{\rm lock} = \gamma_c \sqrt{\frac{|B_{\rm in}|^2}{I_0}}, \tag{39}$$

where γ_c is the cavity decay rate, $|B_{\rm in}|^2$ is the intensity of the input signal, and I_0 is the intensity of the free-running lasing signal in the absence of the input [5]. Within this locking range there is a fixed phase relationship between the input signal and the locked output which varies as

$$\Delta\phi = \arcsin\left[\frac{\omega_{1,\rm free} - \omega_{\rm in}}{\Delta\omega_{\rm lock}}\right]. \tag{40}$$

The same quantity can be calculated in I-SALT and is compared to the Adler prediction for the same slab cavity in the inset of Fig. 1(a). The phase shift variation found from I-SALT is substantially different from the Adler prediction and in good agreement with FDTD [see inset, Fig. 1(b)].

The fact that in this regime the locking transition is entirely due to gain cross saturation, with no contribution from beating or phase synchronization, is illustrated in Fig. 2(a). In the top panel we show the motion of the pole of the scattering matrix corresponding to the lasing mode in Fig. 1 as the pump is increased and then fixed, and then the signal is injected and increased. The dashed blue line corresponds to the laser being below threshold; as the pole moves up towards the real axis its real frequency, ω_1, decreases, pulled toward the center of the atomic line, ω_a. When the pole reaches the real axis, corresponding to the free-running threshold, $\omega_{1,\rm free}$, the gain balances loss and the mode lases. As the pump is further increased, the pole moves slightly further toward the center of the gain curve (not visible on this scale), but as soon as the pump is fixed and the injected signal is turned on at $\omega_{\rm in} < \omega_1$, the behavior reverses. As the injected signal increases, the lasing frequency increases, shifting away from $\omega_{\rm in}$ (and ω_a). Eventually the injected mode saturates the gain enough to drive the lasing mode below threshold, and the pole leaves the real axis, although it continues to be repelled from $\omega_{\rm in}$. This demonstrates that in the regime of stationary atomic populations the locking transition corresponds simply to driving the lasing mode below threshold due to the saturation of the gain medium from the injected mode.

A final important indication of the non-Adler nature of the transition is given in Fig. 2(b). In the Adler theory there are always strong four-wave mixing effects as the locking threshold is reached [5], and additional lines should appear in the frequency spectrum. In Fig. 2(b) we show the Fourier transforms of the FDTD data across the locking transition, which indicated a smooth transfer of intensity from the free-running line to the injected line with no additional frequencies appearing as the free-running line disappears.
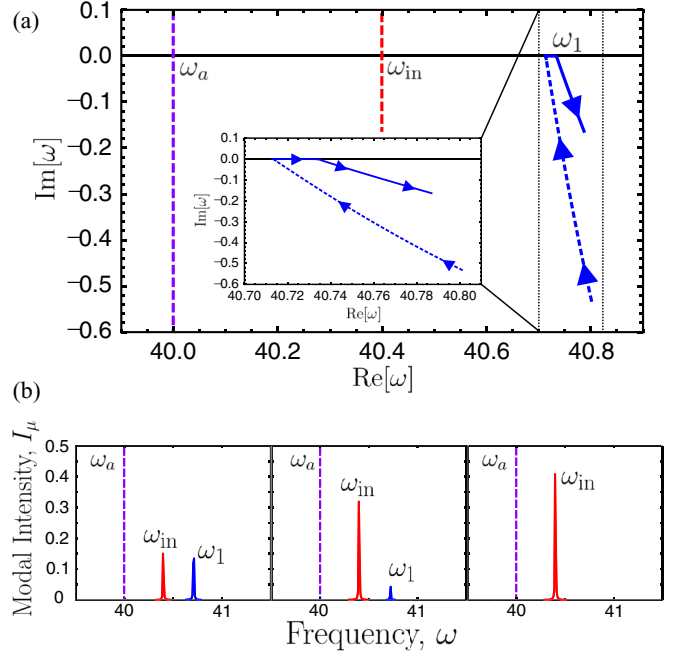

FIG. 2. (Color online) (a) Motion of the pole as described in the text corresponding to the free-running lasing mode in the locking scenario of Fig. 1. As the pump is increased below threshold the pole of the scattering matrix is pulled upwards towards the real axis and "in" towards $\omega_a = 40$ (blue dashed line, recall there is no signal yet at $\omega_{\rm in} = 40.4$). Free-running lasing occurs when the pole reaches the real axis at $\omega_{1,\rm free} = 40.714$ and continues as the pump is increased further above threshold with negligible further frequency shift. Then the pump is fixed and the input signal is ramped, causing the pole (solid blue line) to move to higher frequency, away from the input frequency, and eventually off the real axis as the effects of gain saturation cause the lasing mode to go below threshold. The inset shows a magnification on the motion of the pole of the lasing mode inside the dotted box. (b) Frequency spectrum from FDTD simulations across the locking transition, showing no additional lines appearing, indicating that the effect is purely due to gain cross saturation. Frequencies and rates are given in units of c/L, while the atomic inversion and modal intensities are given in SALT units of E_c and D_c.

B. Partially locked states

Beyond yielding a correct and quantitative treatment of the locking transition of a single-mode laser in the relevant regime, as seen from the generality of Eqs. (21)–(25), I-SALT is able to treat simultaneously multimode lasing with multiple inputs. An interesting example is shown in Fig. 3. Here an asymmetric Fabry-Perot slab laser similar to that in studied in Fig. 1 is pumped above the threshold for its *second* lasing mode (not to be confused with the instability threshold sometimes called the second lasing threshold [7]) and a signal is injected closer to the frequency of the first lasing mode. Because of its stronger interaction with the first mode (blue line), the signal is able to lock that mode, while the second mode (cyan line) remains active at a similar frequency to its free-running value, though shifted away from the injected frequency in the same manner as described before. As before, the solid lines (I-SALT) are in good agreement with the data points (FDTD). Thus,
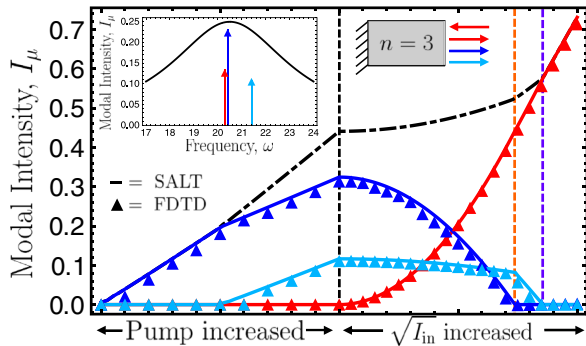
FIG. 3. (Color online) Partial locking transition as described in the text for a laser with two free-running modes and an injected signal (schematic) using a similar pumping and input ramping scheme as Fig. 1, starting at the first lasing threshold $D_0 = 0.101$ and pumping until $D_0 = 0.13$, then increasing the input signal from $B_{in} = 0$ to $B_{in} = 0.4$. Solid lines are output intensities calculated from I-SALT; blue and cyan lines are lasing output, the red line is amplified output at signal frequency, $\omega_{in} = 20.3$, the dot-dashed black line is total output. Triangles are the same quantities from FDTD for a similar dielectric slab laser with $n = 3$, $\omega_a = 20.5$, $\gamma_\perp = 3$, $\gamma_\parallel = 0.001$. The inset shows the relationship of the three frequencies. As expected, the lasing mode nearest to the injected signal locks to the injected signal (orange line), then the more distant lasing mode locks (purple line). Frequencies and rates are given in units of c/L, while the atomic inversion and modal intensities are given in SALT units of E_c and D_c.

with relatively little additional computational effort, I-SALT predicts such "partially locked" states.

C. I-SALT and Adler I-SALT below threshold

The previous results assumed rather large detuning and hence relatively large injected signals to reach locking. To test our work in the more conventional regime of small detuning and small injected signals we consider injection near the free-running lasing frequency as a function of pump. Here we are near the center of the gain spectrum and will have much higher amplification. Since I-SALT is not reliable in the unlocked regime for detuning smaller than the relaxation oscillation frequency, we study only the behavior for pump values below the lasing threshold, when the cavity is functioning as a regenerative amplifier for the injected signal. Since there is only emission at the injected signal in this regime, we can also apply the Adler approximation to I-SALT. As shown in Fig. 4, even though I-SALT may not describe well the unlocked regime for this cavity, it provides a very accurate description of the amplifier, in good agreement with FDTD for both intensity and phase offset. We also find, as one might expect, that the Adler approximation to I-SALT (red curves) works almost as well. The dashed vertical lines in the figure show the lasing thresholds in the absence of the injected signal (orange) and in its presence (purple). In the presence of the injected signal, the first lasing threshold is synonymous with the unlocking transition, as this is when the cavity will begin to self-oscillate. Note that the injected signal pushes up the lasing threshold significantly.
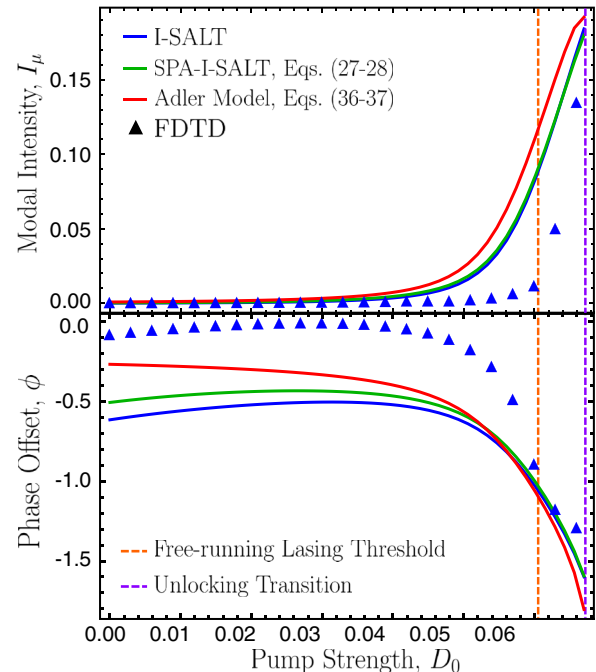

FIG. 4. (Color online) Comparison of the predictions of I-SALT (blue line), the SPA of I-SALT, given by Eqs. (27) and (28) (green line), the Adler model, as given by Eqs. (36) and (37) (red line), and FDTD (blue triangles) for both the output intensity (top) and the phase offset (bottom). The input intensity is negligible ($|B_{in}|^2 = 10^{-4}$ in normalized SALT units) compared to the output, while the pump (gain) is increased from $D_0 = 0$ to $D_0 = 0.067$, thus placing the simulations in the regime of validity for the Adler approximations. The vertical orange dashed line denotes the first lasing threshold in the absence of an incident signal, whereas the vertical purple dashed line shows where I-SALT predicts the unlocking transition to occur. Simulations are shown for a single-sided dielectric slab cavity with $n = 1.5$, $\omega_a = 40$, $\omega_{in} = 40.7$, $\omega_{1,free} = 40.714$, $\gamma_\perp = 4$, and $\gamma_\parallel = 0.001$. Frequencies and rates are given in units of c/L, while the atomic inversion and modal intensities are given in SALT units of E_c and D_c.

D. Injected quadrupole resonators

As noted in our Introduction, a strength of the SALT and I-SALT theories is that they can handle an arbitrary cavity geometry essentially exactly. Here we demonstrate the power of the method by simulating injected two-dimensional quadrupole resonators, below the first lasing threshold. The boundary of the quadrupole cavity is defined by

$$R(\phi) = R_0[1 + \epsilon \cos(2\phi)], \tag{41}$$

where ϕ is the polar angle, R_0 is the average radius, and ϵ is the deformation parameter. Disk or cylinder resonators of this type have been of interest for some time [36,37] because as a function of the deformation the ray dynamics in the cavity undergoes a transition to chaos, with an attendant change in the emission patterns from the laser modes. For thin disks in three dimensions, strictly speaking, one should treat the diffraction effects in the axial (z) direction; for cylinders many wavelengths long one may treat them as infinite in the z direction and study the $k_z = 0$ mode, which then reduces to this purely two-dimensional scalar problem for either the electric

(TM) or the magnetic (TE) modes. It is slightly simpler to treat the TM case for which the electric field is continuous at the boundary and we will focus on that case here. Both SALT and I-SALT are capable of treating modes of arbitrary polarization [28]. In two dimensions, the boundary condition for the incoming and outgoing TCF states requires matching via continuity from the interior cavity solutions to exterior solutions consisting of a superposition of either incoming or outgoing Hankel functions. The detailed method for doing this has been previously described [38,39], and for brevity we omit it here. As mentioned above, the injection profile must now be defined at the border of the entire two-dimensional cavity, which must then be matched to an expansion of the incoming TCF states along this boundary.

Unlike the simple injection boundary condition in a single dimension, Eq. (20), in two dimensions there is an infinite variety of injected fields at the boundary and we find that the choice of the injection profile plays a large role in determining the resulting amplified mode profile, as seen in Fig. 5. Here the cavity is injected with three different injection profiles, all at the first lasing mode's free-running frequency. The first lasing threshold in the absence of injection is shown as the orange dashed line and its corresponding mode profile is shown below. When the injected signal is given by the incoming TCF corresponding to the first lasing mode at threshold, the injected signal is amplified dramatically, and the resulting mode profile is nearly identical to that of the threshold lasing mode. However, when the injected signal, still at the same frequency, is chosen to be the incoming TCF corresponding to the second lasing mode, substantially less amplification occurs and the resulting mode profile is very similar to that of the second lasing mode at threshold, even though the difference in frequency between the first and second lasing modes is small compared with the linewidth of the atomic transition, and they have similar thresholds. Finally, when the incoming signal is represented by the incoming TCF state corresponding to the third lasing mode, almost no amplification occurs, and the mode profile does not resemble the third lasing mode. Evidently, the injected mode profile plays a much stronger role in choosing the resulting amplified mode than the injected frequency does. Essentially, the injected profile is playing the role of a coherent pump or seed with a strong selectivity for a given resonance, so that we may think of it as interchanging the thresholds for, e.g., the first and second modes. This qualitative conclusion may have been difficult to guess in the absence of a quantitative theory.

VI. CONCLUSION

In this work we have developed a method of treating the steady-state behavior of a laser with injected signals which gives an exact treatment of both the openness of the cavity and the effects of spatial hole burning. The theory is valid for Class A and B lasers as long as $\gamma_\parallel$ and the relaxation oscillation frequency are sufficiently small compared to the other relevant frequency scales, as discussed in the Introduction. These conditions are typically met in modern microlasers. I-SALT was then shown to predict qualitatively different behavior of the locking transition from previous Adler-like theories which describe the process as one of phase synchronization.
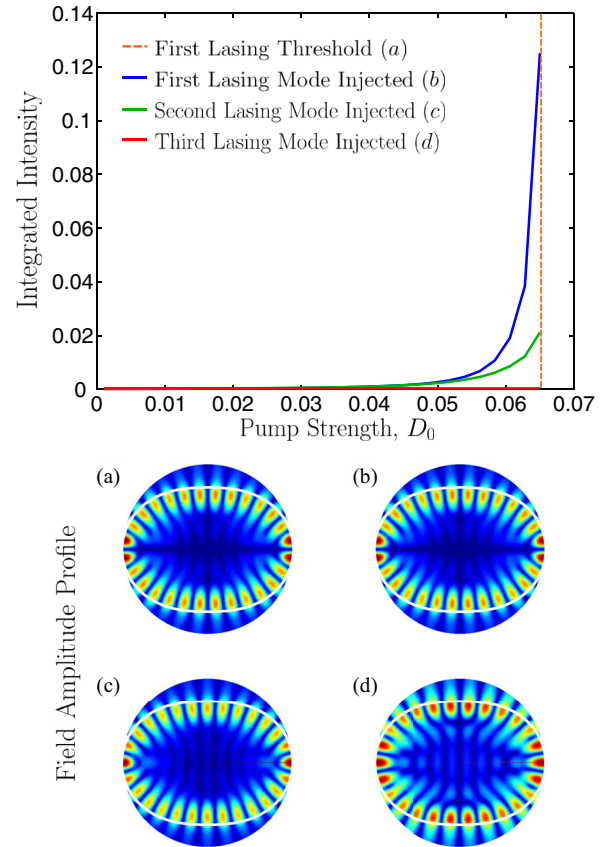

FIG. 5. (Color online) Simulations of a uniform index quadrupole cavity laser amplifier with $n = 1.5$ (boundary indicated in white). The parameters chosen are $R_0 = 1.72~\mu$m, $\lambda_a = 1~\mu$m, $\gamma_\perp = 0.03~\mu$m, and $\epsilon = 0.16$. The injected wavelength for all three simulations is the same as the that for the first free-running mode, $\lambda_{in} = \lambda_1 = 0.989~\mu$m. The pump value was increased from $D_0 = 0$ to the first free-running lasing threshold, $D_0 = 0.065$, vertical orange dashed line. The three solid curves show the amplifier output for three different injection conditions: blue, injection with the TCF corresponding to the first lasing mode; green, injection with the TCF corresponding to the second lasing mode; red, injection with the TCF corresponding to the third lasing mode. Lower plots show in color scale the normalized mode amplitude profiles: (a) The first free-running lasing mode at threshold. (b) The amplified mode with the first lasing mode's incoming TCF as input. (c) The amplified mode with the second lasing mode's incoming TCF as input. (d) The amplified mode with the third lasing mode's incoming TCF as input. The full disk shown in blue is the simulation region used; only TM modes were simulated. The atomic inversion and modal intensities are given in SALT units of E_c and D_c.

When the atomic inversion is stationary, the locking transition is entirely due to spatially varying gain saturation, which has the effect of pushing the frequency of the lasing mode away from the frequency of the injected mode, in contrast to predictions of previous theories. I-SALT can also deal with injection into multimode lasers and predicts partially locked as well as the usual fully locked and free-running states. The theory is designed to treat complex cavity geometries and can easily incorporate different spatial injection profiles into higher dimensional cavities.

The accuracy and stability of the I-SALT theory was confirmed by excellent agreement with brute force FDTD simulations for the case of one-dimensional cavities. However, I-SALT requires substantially less computational effort. For example, I-SALT takes close to an hour of computational time on modern CPUs to generate the curves seen in Fig. 3, while FDTD requires 168 days. In general, exact FDTD studies of multimode lasing are computationally very demanding and could not be performed in more realistic structures, whereas SALT has been shown to be computationally tractable in complex two-dimensional structures such as photonic crystals [23] and random lasers [38], and 3D vectorial codes have been developed [28]. Since I-SALT is essentially of the same degree of computational complexity as SALT, it can be used to predict the effect of injecting signals into such complex modern laser system. This opens up new possibilities for the study of frequency control of both single and multimode lasing and for more general investigations of injected systems. Finally, through comparison between the Adler theory and the approximations made upon I-SALT to rederive this theory, it should be possible to use I-SALT to provide an excellent ansatz to recover time-domain equations similar to those used by previous authors [12–14] for cavities with a complex inner structure, though some care will need to be taken as the spatial profile of the injected signal is a very relevant parameter, as can be seen from the simulations in Sec. V D.

ACKNOWLEDGMENTS

APPENDIX: STABILITY ANALYSIS

The excellent agreement found between I-SALT and FDTD simulations in Sec. V is a good indication that the solutions of I-SALT are stable in time. To confirm this fact, we now perform a stability analysis of the I-SALT solutions under two simplifying assumptions. First, we continue to make the assumption from SALT that the beating terms of the form $\exp[-i(\omega_\sigma - \omega_\nu)t]$ time average to zero, where ω_σ and ω_ν are the frequencies of lasing or amplified modes in the system. Second, we only consider spatially uniform perturbations to the lasing and amplified modes. To address instabilities originating from the beating terms in the inversion equation that are neglected in I-SALT, a different analysis can be performed which is nearly identical to that presented by Ge *et al.* in which the magnitude of the beating the atomic inversion can be calculated [34]. To treat the more general problem of spatially dependent perturbations, a more detailed analysis is being performed by Rotter and Krimer [40]. However, in all previous treatments of stability for injected systems of which we are aware, the slowly varying envelope approximation (SVEA) is invoked, eliminating the spatial degrees of freedom for those treatments as well.

Starting from the Maxwell-Bloch equations, we again insert a modal decomposition of the electric field and polarization,

where the amplitudes have been decomposed into their steady-state values, $\bar{E}, \bar{P}$, and the time-dependent perturbations, $\delta E, \delta P$,

$$E^+ = \sum_\sigma [\bar{E}_\sigma + \delta E_\sigma(t)]\Psi_\sigma(x)e^{-i\omega_\sigma t}, \tag{A1}$$

$$P^+ = \sum_\sigma [\bar{P}_\sigma + \delta P_\sigma(t)]p_\sigma(x)e^{-i\omega_\sigma t}. \tag{A2}$$

The inversion can also be decomposed in a similar manner, but with only the slowly varying part and no "carrier frequency,"

$$D(x,t) = [\bar{D} + \delta D(t)]d(x). \tag{A3}$$

These expansions are then inserted back into the Maxwell-Bloch equations in which we are assuming the cavity dielectric is a constant, the steady-state behavior is removed, and second derivatives of the perturbations are assumed to be much smaller than the other terms, to find

$$4\pi\left(-\omega_\sigma^2 \delta P_\sigma - 2i\omega_\sigma \dot{\delta P}_\sigma\right)p_\sigma(x)$$
$$= \delta E_\sigma\left(\nabla^2 + \varepsilon_c\omega_\sigma^2\right)\Psi_\sigma(x) + 2i\varepsilon_c\omega_\sigma\dot{\delta E}_\sigma\Psi_\sigma(x), \tag{A4}$$

$$\dot{\delta P}_\sigma p_\sigma(x) = (i\omega_\sigma - i\omega_a - \gamma_\perp)\delta P_\sigma p_\sigma(x)$$
$$+ \frac{\gamma_\perp}{4\pi i}(\delta D E_\sigma + D\delta E_\sigma)d(x)\Psi_\sigma(x), \tag{A5}$$

$$\dot{\delta D}d(x) = -\gamma_\parallel\delta D d(x) + 2\pi i\gamma_\parallel$$
$$\times \left[\sum_\sigma(\bar{E}_\sigma\delta P_\sigma^* + \bar{P}_\sigma^*\delta E_\sigma)\Psi_\sigma(x)p_\sigma^*(x) - \text{c.c.}\right]. \tag{A6}$$

The linearized stability equations (A4)–(A6) can be further simplified through the use of the known steady-state solutions,

$$-4\pi\omega_\sigma^2\bar{P}_\sigma p_\sigma(x) = \bar{E}_\sigma\left(\nabla^2 + \varepsilon_c\omega_\sigma^2\right)\Psi_\sigma(x), \tag{A7}$$

$$\bar{P}_\sigma p_\sigma(x) = \frac{\gamma_\sigma}{4\pi}\bar{D}\bar{E}_\sigma d(x)\Psi_\sigma(x), \tag{A8}$$

$$0 = \gamma_\parallel[D_0 - \bar{D}d(x)] + 2\pi\gamma_\parallel i[\bar{E}_\sigma\bar{P}_\sigma^*\Psi_\sigma(x)p_\sigma^*(x) - \text{c.c.}], \tag{A9}$$

which allows for the removal of the spatial profiles of the modes. As such, the evolution of the perturbation of the polarization (A5) can be rewritten by dividing through by $\bar{P}_\sigma p_\sigma(x)$ and using the steady-state solution (A8) to find

$$\frac{\dot{\delta P}_\sigma}{\bar{P}_\sigma} = \frac{i\gamma_\perp}{\gamma_\sigma}\left(\frac{\delta P_\sigma}{\bar{P}_\sigma} - \frac{\delta E_\sigma}{\bar{E}_\sigma} - \frac{\delta D}{\bar{D}}\right). \tag{A10}$$

To simplify the perturbations in the wave equation (A4), one can first evaluate the derivative of the spatial mode profile through the use of the steady-state solution of the wave equation (A7). Next, (A8) is used to rewrite the remaining spatial dependence in terms of the inversion, and finally we integrate both sides with respect to $1/V\int_C d^d x$, resulting in

$$\frac{-2i\varepsilon_c}{\gamma_\sigma\langle\bar{D}d(x)\rangle}\left(\frac{\dot{\delta E}_\sigma}{\bar{E}_\sigma}\right) - 2i\left(\frac{\dot{\delta P}_\sigma}{\bar{P}_\sigma}\right) = \omega_\sigma\left(\frac{\delta P_\sigma}{\bar{P}_\sigma} - \frac{\delta E_\sigma}{\bar{E}_\sigma}\right), \tag{A11}$$

TABLE I. Stability eigenvalues for the cavity shown in Fig. 1 at two different locations of pump and injection strength. The first column shows the eigenvalues right before the injected mode is turned on, with only a single lasing mode active in the cavity. The second column shows the eigenvalues when both the lasing mode and amplified mode are present in the cavity and have nearly the same output intensity. In both cases, the I-SALT solution is found to be stable, though in the second case, an extra marginal eigenvalue is found.

	$D_0 = 0.075$, $B_{in} = 0$	$D_0 = 0.08$, $B_{in} = 0.10$
λ_1	$-4.60878 + 0.70576i$	$-4.61428 + 0.71661i$
λ_2	$-4.60878 - 0.70576i$	$-4.61428 - 0.71661i$
λ_3	-0.00088	-0.00084
λ_4	-0.00012	-0.00016
λ_5	0	0
λ_6		$-4.60483 + 0.34413i$
λ_7		$-4.60483 - 0.34413i$
λ_8		0
λ_9		0

where

$$\langle \bar{D} d(x) \rangle = \frac{1}{V} \bar{D} \int_C d(x) d^d x \qquad (A12)$$

is the spatial average of the inversion. As we are not considering spatially dependent perturbations, only global changes in the amplitudes of the fields in the problem, treating the spatial variation of the inversion would violate our previous assumptions. It should be noted that this spatial average could also be performed at the outset (A4)–(A6) without changing any of these results.

Finally, the evolution of the perturbation in the inversion (A6) can be rewritten using the steady state of the polarization (A8) and its complex conjugate, and again integrating over the cavity, to find

$$\frac{\dot{\delta D}}{\bar{D}} = -\gamma_\parallel \frac{\delta D}{\bar{D}} + \left(\frac{i\gamma_\parallel}{2} \right) \sum_\sigma \langle |\bar{E}_\sigma \Psi_\sigma(x)|^2 \rangle$$

$$\times \left[\gamma_\sigma^* \left(\frac{\delta P_\sigma^*}{\bar{P}_\sigma^*} + \frac{\delta E_\sigma}{\bar{E}_\sigma} \right) - \text{c.c.} \right], \qquad (A13)$$

where

$$\langle |\bar{E}_\sigma \Psi_\sigma(x)|^2 \rangle = \frac{1}{V} \int_C |\bar{E}_\sigma \Psi_\sigma(x)|^2 d^d x \qquad (A14)$$

is the spatial average of the lasing mode profile.

The evolution equations for the perturbations, (A10), (A11), and (A13), collectively comprise $4(N_L + N_A) + 1$

independent equations, four equations per mode for the real and imaginary portions of (A10) and (A11), and a single real equation for the perturbation to the atomic inversion (A13), which couples all of the active modes together. The last step, which is standard in a stability analysis calculation, is to assume solutions of these equations in the form

$$\delta E_\sigma, \delta P_\sigma, \delta D \propto e^{\lambda t} \qquad (A15)$$

and ensure that all of the solutions are decaying, $\text{Re}[\lambda] < 0$. However, in the case of a lasing mode there is an undetermined global phase of the mode; thus, for every lasing mode in the calculation we expect a single marginal eigenvalue, $\text{Re}[\lambda] = 0$, corresponding to the lack of a restoring force for the phase of the lasing mode. We also expect a single marginal eigenvalue for each amplified mode as well. This is a reflection of the fact that the amplitude perturbation of an injected mode being considered here is affecting both the incoming and the outgoing portions of the mode equally,

$$\delta E_\alpha(t) \Psi_\alpha(x) = \delta E_\alpha(t) \left[\sum_n a_n^{(\alpha)} u_n(x; \omega_\alpha) \right.$$
$$\left. + \sum_m b_m^{(\alpha)} v_m(x; \omega_\alpha) \right], \qquad (A16)$$

and thus has the ability to change the global phase of both the incoming and the outgoing components of the mode. However, it must alter both portions by the same phase shift, thus leaving the relative phase difference between the incident and the outgoing components fixed, as is expected.

The results for this spatially averaged stability analysis for the simulations shown in Fig. 1 can be seen in Table I. The first column shows the eigenvalues for the cavity when only a single lasing mode is active, right before the pump is fixed and the incident mode is turned on, and the I-SALT solution is found to be stable. As expected, we find four decaying eigenvalues and a single marginal eigenvalue. The second column shows the eigenvalues for the cavity when both the lasing and the amplified modes are present in the cavity at nearly the location where their output intensities are equal. Again, the I-SALT solution found is stable, with only decaying or marginal eigenvalues found; however, an extra marginal eigenvalue is found, which was not anticipated. The analysis of why there is an extra marginal eigenvalue is left for the future, more complete stability analysis of the SALT and I-SALT solutions.

[1] R. Pantell, Proc. Inst. Electr. Eng. **53**, 474 (1965).

[2] C. L. Tang and H. Statz, J. Appl. Phys. **38**, 323 (1967).

[3] R. Boikova and E. Fradkin, Opt. Spectrosc. (USSR) **22**, 452 (1967).

[4] M. B. Spencer and W. E. Lamb, Phys. Rev. A **5**, 884 (1972).

[5] A. E. Siegman, *Lasers* (University Science, Mill Valley, CA, 1986).

[6] R. Adler, Proc. IRE **34**, 351 (1946).

[7] H. Haken, *Light: Laser Dynamics* (North-Holland Physics, New York, 1985), Vol. 2.

[8] J. Ohtsubo, *Semiconductor Lasers: Stability, Instability, and Chaos* (Springer, New York, 2007).

[9] S. Wieczorek, B. Krauskopf, T. B. Simpson, and D. Lenstra, Phys. Rep. **416**, 1 (2005).

[10] F. T. Arecchi, G. L. Lippi, G. P. Puccioni, and J. R. Tredicce, Opt. Commun. **51**, 308 (1984).

[11] F. Mogensen, H. Olesen, and G. Jacobsen, IEEE J. Quantum Electron. **21**, 784 (1985).

[12] G. L. Oppo, A. Politi, G. L. Lippi, and F. T. Arecchi, Phys. Rev. A **34**, 4000 (1986).

[13] H. G. Solari and G. L. Oppo, Opt. Commun. **111**, 173 (1994).

[14] M. G. Zimmermann, M. A. Natiello, and H. G. Solari, Chaos **11**, 500 (2001).

[15] B. Kelleher, S. P. Hegarty, and G. Huyet, Phys. Rev. E **86**, 066206 (2012).

[16] R. Lang, IEEE J. Quantum Electron. **18**, 976 (1982).

[17] C. Henry, IEEE J. Quantum Electron. **18**, 259 (1982).

[18] C. Henry, J. Lightwave Technol. **4**, 288 (1986).

[19] P. Even, K. Ait Ameur, and G. M. Stéphan, Phys. Rev. A **55**, 1441 (1997).

[20] E. G. Lariontsev, I. Zolotoverkh, P. Besnard, and G. M. Stéphan, Eur. Phys. J. D **5**, 107 (1999).

[21] S. L. McCall, A. F. J. Levi, R. E. Slusher, S. J. Pearton, and R. A. Logan, Appl. Phys. Lett. **60**, 289 (1992).

[22] D. K. Armani, T. J. Kippenberg, S. M. Spillane, and K. J. Vahala, Nature (London) **421**, 925 (2003).

[23] S. Chua, Y. D. Chong, A. D. Stone, M. Soljačić, and J. Bravo-Abad, Opt. Express **19**, 1539 (2011).

[24] X. Jiang, S. Feng, C. M. Soukoulis, J. Zi, J. D. Joannopoulos, and H. Cao, Phys. Rev. B **69**, 104202 (2004).

[25] Y. D. Chong and A. D. Stone, Phys. Rev. Lett. **109**, 063902 (2012).

[26] A. Pick, A. Cerjan, A. W. Rodriguez, Y. D. Chong, A. D. Stone, and S. G. Johnson (unpublished).

[27] A. Cerjan, Y. D. Chong, L. Ge, and A. D. Stone, Opt. Express **20**, 474 (2012).

[28] S. Esterhazy, D. Liu, M. Liertzer, A. Cerjan, L. Ge, K. G. Makris, A. D. Stone, J. M. Melenk, S. G. Johnson, and S. Rotter, arXiv:1312.2488 [Phys. Rev. A (to be published)].

[29] H. Fu and H. Haken, Phys. Rev. A **43**, 2446 (1991).

[30] A. Cerjan, Y. D. Chong, and A. D. Stone, arXiv:1406.6659.

[31] L. Ge, Y. D. Chong, and A. D. Stone, Phys. Rev. A **82**, 063824 (2010).

[32] H. E. Türeci, A. D. Stone, and L. Ge, Phys. Rev. A **76**, 013813 (2007).

[33] B. Bidégaray, Numer. Methods Partial Differ. Equations **19**, 284 (2003).

[34] L. Ge, R. J. Tandy, A. D. Stone, and H. E. Türeci, Opt. Express **16**, 16895 (2008).

[35] A. Murakami, K. Kawashima, and K. Atsuki, IEEE J. Quantum Electron. **39**, 1196 (2003).

[36] J. U. Nöckel and A. D. Stone, Nature (London) **385**, 45 (1997).

[37] C. Gmachl, F. Capasso, E. E. Narimanov, J. U. Nöckel, A. D. Stone, J. Faist, D. L. Sivco, and A. Y. Cho, Science **280**, 1556 (1998).

[38] H. E. Türeci, L. Ge, S. Rotter, and A. D. Stone, Science **320**, 643 (2008).

[39] L. Ge, Ph.D. thesis, Yale University, New Haven, CT, 2010.

[40] D. Krimer and S. Rotter (private communication).